第8卷 第1期 物理化学学报 Vol.8, No.1
1992年2月 ACTA PHYSICO-CHIMICA SINICA Feb., 1992

MODELING SIMULATION OF SECONDARY PROCESSES IN PHOTOFRAGMENT-TRANSLATIONAL SPECTROSCOPY

Zhao Xinsheng*
(Department of Chemistry, Peking University Beijing 100871, China)

Nathanson, Gilbert M.
(Department of Chemistry, University of Wisconsin, Madison, WI 53706, USA)

Lee, Yuan T.
(Materials and Chemical Sciences Division, Lawrence Berkeley Laboratory and Department of Chemistry, University of California, Berkeley, CA94720, USA)

We developed a method for analyzing time-of-flight spectra of Secondary products from sequential dissociation reactions following photon absorption by the parent molecule. This work complements the original discussion by Kroger and Riley, and shows that substantial information can be extracted even from highly aveyaged data. This information includes the average translational energy release and anisotropy of the secondary product recoil, as well as the relative yields of the secondary fragments for competing pathways. Model results are examined in order to illustrate the basic features of secondary dissociation.

Keywords Data simulation, photodissociation, molecular beam, Secondary process

Molecules that are activated through photon absorption can often decompose along different pathways. After initial dissociation, the recoiling fragments may contain enough energy to fall apart, or they may absorb an additional photon and then dissociate.

In photofragment-translational spectroscopy (PTS) experiments[1], the incident supersonic molecular beam is translationally and rotationally cold and highly collimated. The parent molecules are confined to a narrow range of energies and momenta.

Manuscript received 1990-11-29; revised manuscript received 1991-04-10.

The conditions differ substantially for secondary dissociation, since the primary products become the new reactants. In addition, the primary fragment velocities and directions normally span the full limit imposed only by energy and momentum conservation during dissociation. Simultaneous fits to the TOF spectra of the momentum matched primary and secondary fragments, however, are often severely constrained by the reaction dynamics, and energy and angular distributions, as well as branching ratios for different decay paths, can be extracted from the data. We have followed this procedure in analyzing the secondary decomposition of RDX [2], alkyl acetates [3], and in determining the existence of potential and rotational barriers in concerted reactions [4].

In the sections below, we describe one approach toward analyzing secondary dissociation processes in PTS experiments. This work is preceded by previous calculations of Kroger and Riley [5]. They also showed how to discriminate between sequential and simultaneous three-body dissociation [6]. Recently, Vernon and coworkers [7] have used a statistical model to fit the sequential elimination of CO from $Fe(CO)_5$. The fundamental relations for crossed beam experiments were discussed in depth by warnock and Bernstein [8] and by Pack [9]. Our analysis focuses on secondary dissociation in PTS experiments. A detailed discussion of state-to-state reactions in a general PTS experimental setup has been given by Zhao [10]. In Sec. I we will outline a simplified version of the results obtained in Ref [10]. In Sec. II we introduce further approximations to carry out the simulation, and then give examples to display some features of secondary dissociation.

I · KINETICS AND KINEMATICS

A. Chemical Kinetics

Spontaneous secondary dissociation follows a three-step, sequential process:

$$R + h\nu \xrightarrow{k_\nu} R^*,$$

$$R^* \xrightarrow{k_n^d} A_n + B_n, \qquad n = 1 \text{ to } p$$

and

$$A_n \xrightarrow{k_{nm}^d} G_{nm} + H_{nm} \qquad m = 1 \text{ to } q$$

R and R* are the initial and energized parent molecules respectively, A_n and B_n are the products of the n^{th} primary channel, and G_{nm} and H_{nm} are the products of the n^{th} primary and m^{th} secondary paths. Approximate rate equations which avoid the labeling of internal states are:

initial R

$$\frac{dn_R(v_R, w_R, t)}{dt} = -k_\nu I(t) n_R(v_R, w_R, t) \tag{1}$$

energized R*

$$\frac{dn_R^*(v_R,w_R,t)}{dt} = k_v I(t) n_R(v_R, w_R, t)$$

$$- \sum_n \int k_n^d(R^* \rightarrow E_{Tn}, \Omega_n) dE_{Tn} d\Omega_n n_R^*(v_R, w_R, t) \quad (2)$$

Primary products that dissociate

$$\frac{dn_{An}(E_{Tn}, \Omega_n, t)}{dt} = \int k_n^d(R^* \rightarrow E_{Tn}, \Omega_n) n_R^*(v_R, w_R, t) dv_R dw_R$$

$$- \sum_{nm} \int k_{nm}^d(E_{Tn}, \Omega_n \rightarrow E_{Tnm}, \Omega_{nm}) dE_{Tnm} d\Omega_{nm} n_{An}(E_{Tn}, \Omega_n, t) \quad (3)$$

secondary products

$$\frac{dn_{Gnm}(v_{Gnm}, w_{Gnm}, t)}{dt} =$$

$$\int_{\{v_{Gnm}, w_{Gnm}\}} k_{nm}^d(E_{Tn}, \Omega_n \rightarrow E_{Tnm}, \Omega_{nm}) n_{An}(E_{Tn}, \Omega_n, t) dE_{Tn} d\Omega_n dE_{Tnm} d\Omega_{nm} \quad (4)$$

$n_Y(x,y,z)$ is the number density of species Y as function of x, y, and z, and v_Y and w_Y are the LAB velocity and solid angle for species Y. The bracket { } indicates quantities that are fixed during integration or summation. I(t) is the intensity of the light. k_v is the electric dipole absorption rate constant, which depends on $|<\hat{\mu}\cdot\hat{\epsilon}>|^2$, where $\hat{\mu}$ and $\hat{\epsilon}$ are the unit vectors of the transition dipole of the parent molecule and the electric field of the radiation. $k_n^d(R^* \rightarrow E_{Tn}, \Omega_n)$ is the rate constant for primary dissociation from R* at v_R and w_R yielding products A_n and B_n with center-of-mass (c. m.) translational energy E_{Tn} traveling into c. m. solid angle Ω_n. $k_{nm}^d(E_{Tn}, \Omega_n \rightarrow E_{Tnm}, \Omega_{nm})$ is the analogous rate constant for secondary dissociation.

We introduce the effective reaction time τ which is determined by the length of the laser pulse and the lifetime of the energized molecules such that decomposition is essentially complete at time τ. The integration of Eqn. (3) can be rearranged to give

$$\int_0^\tau n_{An}(E_{Tn}, \Omega_n, t) dt = \frac{\int dv_R dw_R k_n^d(R^* \rightarrow E_{Tn}, \Omega_n) \int_0^\tau n_R^*(v_R, w_R, t) dt}{\sum_m \int dE_{Tnm} d\Omega_{nm} k_{nm}^d(E_{Tn}, \Omega_n \rightarrow E_{Tnm}, \Omega_{nm})} \quad (5)$$

where $\int_0^\tau n_R^*(v_r, w_r, t)\, dt$ is in turn determined from the integration of Eqns. (1) and (2). Thus, at low light intensity the velocity distribution in the laboratory frame for the total number of secondary products after the laser pulse is

$$N_{Gnm}(v_{Gnm}, w_{Gnm})\mathrm{d}v_{Gnm}\mathrm{d}w_{nm} =$$

$$VI_0\int_{\{v_{Gnm}, w_{Gnm}, \mathrm{d}v_{Gnm}, \mathrm{d}w_{nm}\}} \mathrm{d}E_{Tn}\mathrm{d}\Omega_n\mathrm{d}E_{Tnm}\mathrm{d}\Omega_{nm}\mathrm{d}v_R\mathrm{d}w_R n_R^0(v_R, w_R) \cdot$$

$$\frac{k_{nm}^d(E_{Tn}, \Omega_n \rightarrow E_{Tnm}, \Omega_{nm})}{\sum_m \int \mathrm{d}E_{Tnm}\mathrm{d}\Omega_{nm} k_{nm}^d(E_{Tn}, \Omega_n \rightarrow E_{T\,nm}, \Omega_{nm})} \cdot \frac{k_n^d(R^* \rightarrow E_{Tn}, \Omega_n)k_r}{\sum_n \int k_n^d(R^* \rightarrow E_{Tn}, \Omega_n)\mathrm{d}E_{Tn}\mathrm{d}\Omega_n} \tag{6}$$

where V is the effective volume of the interaction region, $n_R^0(v_R, w_R)$ is the initial density of R, and

$$I_0 = \int_0^\tau I(t)\mathrm{d}t \tag{7}$$

is the fluence of light. Note that the numerator is integrated according to the bracketed constraints, while the integral in the denominator is over all possible (E_{Tn}, Ω_n) and (E_{Tnm}, Ω_{nm}). These constraints limit the integration within the range v_{Gnm} to $v_{Gnm} + \mathrm{d}v_{Gnm}$ and w_{nm} to $w_{nm} + \mathrm{d}w_{nm}$. This is shown in the velocity space or "Newton" diagram for secondary dissociation in Fig. 1, where the constraints are imposed on the sun of velocity vectors that connect the vicinity of the point G_{nm} with LAB velocity v_{Gnm}. A second fundamental constraint is imposed by energy conservation.

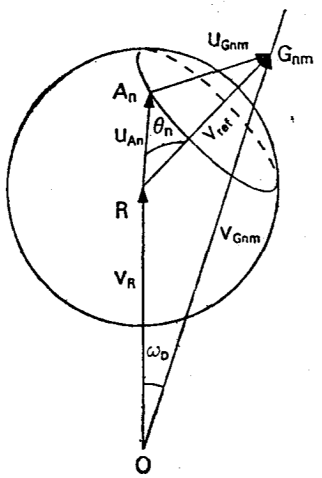

Fig. 1 Kinematic relations for secondary dissociation. O is the origin of the LAB frame, OR is the direction of the molecular beam, and OG_{nm} is the line of detection. u_{An} and u_{Gnm} are the recoil velocity vector for the primary A_n and secondary G_{nm} products. Other symbols are explained in the text.

The products on the right hand side of Eqn. (6) divide naturally into two terms describing primary and secondary dissociation. These are

$$P_n(E_{Tn},\ \Omega_n)=\frac{VI_0k_n^d(R^*\rightarrow E_{Tn},\ \Omega_n)k,}{\sum_n\int k_n^d(R^*\rightarrow E_{Tn},\ \Omega_n)dE_{Tn}d\Omega_n}\cdot\frac{1}{C_n(R)} \tag{8}$$

where

$$C_n(R)=\frac{VI_0\int k_n^d(R^*\rightarrow E_{Tn},\ \Omega_n)k,dE_{Tn}d\Omega_n}{\sum_n\int k_n^d(R^*\rightarrow E_{Tn},\ \Omega_n)dE_{Tn}d\Omega_n} \tag{9}$$

and

$$P_{nm}(E_{Tn},\ \Omega_n,\ E_{Tnm},\ \Omega_{nm})=$$

$$\frac{k_{nm}^d(E_{Tn},\ \Omega_n\rightarrow E_{Tnm},\ \Omega_{nm})}{\sum_m\int E_{Tnm}d\Omega_{nm}k_{nm}^d(E_{Tn},\ \Omega_n\rightarrow E_{Tnm},\ \Omega_{nm})}\cdot\frac{1}{C_{nm}(E_{Tn},\ \Omega_n)} \tag{10}$$

where

$$C_{nm}(E_{Tn},\ \Omega_n)=\frac{\int dE_{Tnm}d\Omega_{nm}k_{nm}^d(E_{Tn},\ \Omega_n\rightarrow E_{Tnm},\ \Omega_{nm})}{\sum_m\int dE_{Tnm}d\Omega_{nm}k_{nm}^d(E_{Tn},\ \Omega_n\rightarrow E_{Tnm},\ \Omega_{nm})} \tag{11}$$

Notice that according to the above definitions, we have

$$\int P_n(E_{Tn},\ \Omega_n)dE_{Tn}d\Omega_n=1 \tag{12}$$

and

$$\int P_{nm}(E_{Tn},\ \Omega_n,\ E_{Tnm},\ \Omega_{nm})dE_{Tnm}d\Omega_{nm}=1 \tag{13}$$

With these definitions, the new expression for N_{Gnm} is

$$N_{Gnm}(v_{Gnm},\ w_{Gnm})dv_{Gnm}dw_{nm}=$$

$$\int_{(v_{Gnm},w_{Gnm},dv_{Gnm},dw_{Gnm})}dE_{Tn}d\Omega_ndE_{Tnm}d\Omega_{nm}dv_Rdw_RC_n(R)C_{nm}(E_{Tn},\ \Omega_n)P_n(E_{Tn},\ \Omega_n)\cdot$$

$$P_{nm}(E_{Tn},\ \Omega_n,\ E_{Tnm},\ \Omega_{nm})n_R^0(v_R,\ w_R) \tag{14}$$

$P_n(E_{Tn},\ \Omega_n)$ is the normalized probability for creating primary products which dissociate, with c. m. translational energy E_{Tn} traveling into c. m. solid angle Ω_n. $P_{nm}(E_{Tn},\ \Omega_n,\ E_{Tnm},\ \Omega_{nm})$ is the analogous probability for secondary dissociation normalized with respect to E_{Tnm} and Ω_{nm}. $C_{nm}(E_{Tn},\ \Omega_n)$ determines the fraction of events through the m^{th} secondary channel out of all secondary channels from the same primary product A_n at the sample point E_{Tn} and Ω_n.

The total number of secondary products G_{nm} is

$$N_{Gnm}^{tot}=\int dE_{Tn}d\Omega_ndv_Rdw_RdE_{Tnm}d\Omega_{nm}C_n(R)P_n(E_{Tn},\ \Omega_n)\cdot$$

$$C_{nm}(E_{Tn},\Omega_n)P_{nm}(E_{Tn},\Omega_n,E_{Tnm},\Omega_m)n_R^0(v_R,w_R)$$
$$=C_n(R)C_{nm}(R)n_0 \tag{15}$$

where n_0 is the density of parent molecules in the interaction zone. In order to obtain Eqn. (15), we need to assume that $C_{nm}(E_{Tn},\Omega_n)$ is independent of E_{Tn} and Ω_n. The branching ratio between two channels is defined to be the ratio of the total number of products produced under the same experimental conditions, corrected by the moles of reaction. By fitting the experimental data, $C_n(R)$ and $C_{nm}(R)$ can be obtained for the branching ratio calculation[10,11].

B. Kinematic relations

PTS experiments measure the number of ion counts $N_{Gnm}^{T+}(T,w_D)$ at laboratory angle w_i, as a function of time T after the laser pulse.

The reaction products in our PTS setup[1] are detected by electron impact ionization in the limit where the ionization probability is inversely proportional to the LAB velocity of the product,

$$N_{Gnm}^{T+}(T,w_D)=\frac{\eta_{Gnm}}{v_{Gnm}}N_{Gnm}^{T}(T,w_D) \tag{16}$$

In the experimentally interested range of v_{Gnm}, it is found that setting η_{Gnm} to a constant η_{Gnm}^0 is a good approximation. The simulated product TOF spectrum is obtained from

$$N_{Gnm}^{T}(T,w_D)\,dT=\left[\int_{(w_D)}N_{Gnm}(v_{Gnm},w_{Gnm})\left|\frac{\delta v_{Gnm}}{\delta T}\right|dw_{Gnm}\right]dT \tag{17}$$

where, from $v_{Gnm}=L/T$; $\left|\frac{\delta v_{Gnm}}{\delta T}\right|=\frac{v_{Gnm}}{T}$

The expression for $N_{Gnm}(v_{Gnm},w_{Gnm})\,dv_{Gnm}dw_{nm}$ is transformed from c. m. translational energies to LAB velocities using the relations

$$E_{Tn}=\tfrac{1}{2}\frac{M_RM_{An}}{M_{Bn}}u_{An}^2 \quad \text{and} \quad E_{Tnm}=\tfrac{1}{2}\frac{M_{An}M_{Gnm}}{M_{Hnm}}u_{Gnm}^2$$

and the integral transformation

$$\frac{\partial(u_{Gnm},\Omega_{nm})}{\partial(v_{Gnm},w_{Gnm})}=\frac{v_{Gnm}^2}{u_{Gnm}^2}$$

Substituting these relations into Eqns. (14), (16) and (17) yields

$$N_{Gnm}^{T+}(T,w_D)=$$
$$\eta_{Gnm}^0C_{nm}(R)C_n(R)\frac{v_{Gnm}^2}{T}\frac{M_RM_{An}}{M_{Bn}}\frac{M_{Gnm}M_{An}}{M_{Hnm}}\int_{(T,w_D)}du_{An}d\Omega_{An}dv_Rdw_Rdw_{Gnm}\cdot$$
$$P_n(E_{Tn},\Omega_n)u_{An}\frac{P_{nm}(E_{Tn},\Omega_n,E_{Tnm},\Omega_{nm}}{u_{Gnm}}n_R^0(v_R,w_R) \tag{18}$$

This equation relates the measured number of ion counts $N^{T+}_{Gnm}(T, w_D)$ to the primary and secondary probability distributions, which can be obtained by forward convolution fitting procedures. When necessary, Eqn. (18) should be averaged over the finite interaction and ionization zones. In the next section, further approximations are introduced to make the data analysis simpler.

II. FURTHER APPROXIMATIONS AND EXAMPLES

A. Product probability distributions

Experiments have demonstrated that the factorization of

$$P_n(E_{Tn}, \Omega_n) = P_{\Omega n}(\Omega_n) \cdot P_{En}(E_{Tn})$$

is acceptable when the parent molecules have been cooled by supersonic expansion. The angular distribution of primary products for dipole-allowed transition was shown by Zare[12] to be

$$P_{\Omega n}(\Omega_n) = (1/4\pi)(1 + \beta_n P_2(\hat{u}_{An} \cdot \hat{\epsilon})) \tag{19}$$

where $P_2(x)$ is the second Legendre polynomial of x, and β_n is the anisotropy parameter for the n^{th} primary channel, equal to values between 2 and -1. The limits of 2 and -1 are reached for direct, repulsive dissociations parallel and perpendicular to the transition dipole $\hat{\mu}$, respectively.[12]

In the case of secondary spontaneous dissociation, the dependence of $P_{nm}(E_{Tn}, \Omega_n, E_{Tnm}, \Omega_{nm})$ on Ω_n is negligible, and we assume that it can also be factored into

$$P_{nm}(E_{Tn}, \Omega_n, E_{Tnm}, \Omega_{nm}) = P_{\Omega nm}(\Omega_{nm}) \cdot P_{Enm}(E_{Tn} \rightarrow E_{Tnm})$$

The c. m. velocity distribution of the secondary fragments depends on the internal energy of the decomposing primary fragment. When B_n in the primary process is an atom, the internal energy of A_n can be accurately obtained by subtracting E_{Tn} from the available energy of the primary process, and analytical functions, such as given by RRKM theory, can be used for $P_{Enm}(E_{Tn} \rightarrow E_{Tnm})$[4]. However, when the internal energy of an individual species at E_{Tn} cannot be determined or when a proper analytic function for $P_{Enm}(E_{Tn} \rightarrow E_{Tnm})$ is not available, a further assumption is made that $P_{Enm}(E_{Tn} \rightarrow E_{Tnm})$ is independent of E_{Tn}. This severe approximation is often justified by the fact that in lots of cases the translational energy distribution is not a sensitive function of the internal energy of the reactant, and by the substantial averaging that occurs during secondary dissociation.

The separation of the angular and energy variables allows the integral over the azimuthal angle ϕ_n in the double differential $d\Omega_n = \sin\theta_n d\theta_n d\phi_n$ to be performed analytically for spontaneous secondary dissociation. This is shown pictorially in the velocity diagram in Fig. 1. For fixed values of the c. m. and LAB velocities, those recoiling primary products which lie on the cut of the primary sphere and contribute to detected signal at w_D and v_{Gnm} are centered on the reference line v_{ref}. When the u_z axis is chosen along v_{ref} for the primary variables, the azimuthal integral of

$P_{Qn(\Omega_n)}$ in Eqn. (19) can be performed analytically to give

$$\int P_{Qn}(\Omega_n)\mathrm{d}\phi_n = \int (1/4\pi)(1+\beta_n P_2(\hat{u}_{An}\cdot\hat{\epsilon}))\mathrm{d}\phi_n$$

$$= 1/2 \cdot (1+\beta_n P_2(\cos\theta_n) P_2(\hat{v}_{ref}\cdot\hat{\epsilon})) \tag{20}$$

since all the other variables are fixed during the integration[13].

With the approximations described above, Eqn. (18) yields the final relation used in data analysis:

$$N^{T+}_{Gnm}(T, w_D) =$$

$$\eta^{\circ}_{Gnm} C_{nm}(R) C_n(R) \frac{v^2_{Gnm}}{T} \frac{M_R M_{An}}{M_{Bn}} \frac{M_{Gnm} M_{An}}{M_{Hnm}} \int_{(T,w_D)} \mathrm{d}u_{An} \sin\theta_n \mathrm{d}\theta_n \mathrm{d}v_R \mathrm{d}w_R \mathrm{d}w_{Gnm} \cdot$$

$$1/2 \cdot (1+\beta_n P_2(\cos\theta_n) P_2(\hat{v}_{ref}\cdot\hat{\epsilon})) \cdot P_{En}(E_{Tn}) u_{An} \cdot n^0_R(v_R, w_R) \cdot$$

$$\frac{P_{Enm}(E_{Tnm}) P_{Qnm}(\Omega_{nn})}{u_{Gnm}} \tag{21}$$

The treatment on secondary photodissociation has been discussed in detail in Ref. 10.

B. Examples

The reliability of Eqn. (21) has been intensively investigated by both model simulations and application to the analysis of real PTS experiments[2-4, 10].

In the following model simulation we take $v_R = 1.40\times10^5$ cm·s^{-1}, typical for a supersonic beam with helium as the carrier gas. The flight path L is assumed to be 35 cm.

Fig. 2 shows the model primary and secondary translational energy distributions for a parent molecule of 200 amu dissociating into two fragments of 100 amu each, followed by spontaneous dissociation of one of the primary products into fragments of 35 and 65 amu. These translational energy distributions correspond to the most probable velocities of $u_{100} = 8.00\times10^4$ cm·s^{-1} in the primary c. m. reference frame, and $u_{35} = 8.00\times10^4$ cm·s^{-1} and $u_{65} = 4.31\times10^4$ cm·s in the secondary c. m. reference frame.

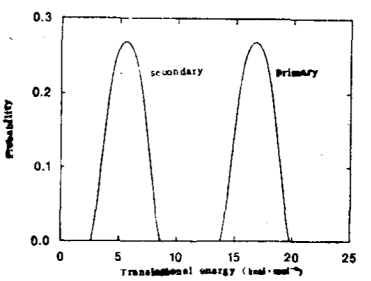

Fig. 2 Primary and secondary translational energy distributions used in the simulation

Fig. 3 shows diagrams of a cut through the plane of the molecular beam and line of detection in velocity space for the most probable velocities corresponding to Fig. 2. The dashed circles represent the velocities of the primary products, and the

solid circles indicate the recoil velocities of the secondary products. The coalescence of the circles at the inner and outer rims of the figures are often observed in PTS experiments [4, 14].

Fig. 4 shows the TOF spectra of the primary products which do not dissociate. Notice the narrow, forward peaks at most LAB angles. At 35° the line of detection just cuts through the edge of the most probable primary velocity circle, and the peaks due to forward and backward scattering merge together, making this TOF distribution the broadest.

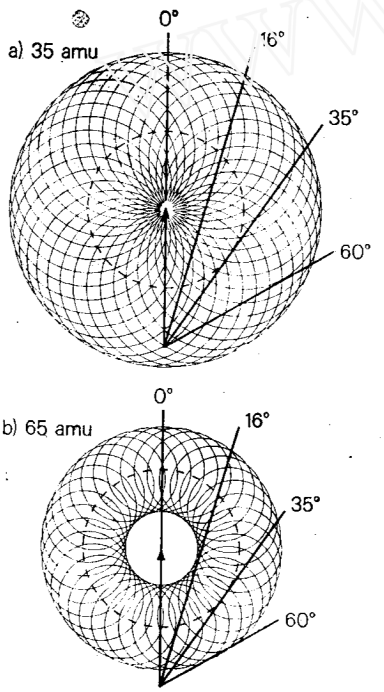

Fig. 3 An in-plane cut through the "Newton" diagram of Fig.1 showing the most probable velocity corresponding to the translational energy distributions in Fig.2 The heavy solid lines are the detection axes, the dashed circles represent the recoil velocities of the primary 100 amu product, and the solid circles are the recoil velocities for the secondary 35 and 65 amu species

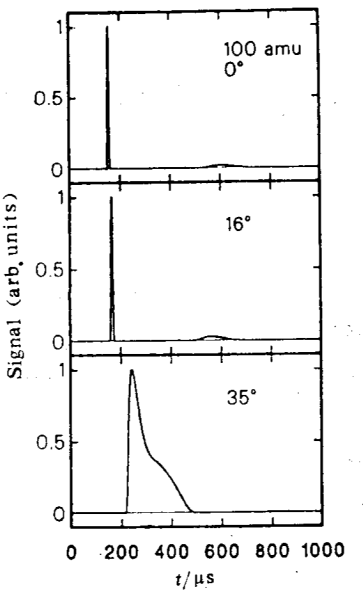

Fig. 4 TOF spectra of the primary 100 amu product at different LAB angles

Figs. 5 and 6 show TOF spectra of the secondary products when both primary and secondary processes are isotropic. The buildup in signal along the rims of the secondary circles is clearly shown in the TOF spectra at 0° and 16°. The fast peak is signal originating from the outer rim of the Newton diagram, and the next peak or bump at 0° or 16° is from the inner rim.

Anisotropic primary dissociation can be observed in some systems when the laser is polarized. This anisotropy is reflected even in the secondary TOF spectra, and is clearly shown in Fig. 7 for the 35 amu species with the laser polarization vector $\hat{\epsilon}$ along the line of detection. For $\beta_n = 2$, the sharp, doubly peaked spectrum is obtained because the primary recoil is focussed in the forward (fast times) and backward (slow times) directions of the Newton diagram. The opposite effect is observed for $\beta_n = -1$ because primary dissociation is intensified perpendicular to $\hat{\epsilon}$ and has little intensity in the forward and backward directions.

When the secondary dissociation is anisotropic the TOF spectra may become even more structured. Fig. 8 shows the TOF spectra of 35 amu species at 16° with two secondary angular distributions, while the primary process is assumed isotropic. Fig. 8 a) is a simulation using

$$P_{\Omega nm}(\Omega_{nm}) = A/\sin\theta_{nm} \qquad \pi/36 < \theta_{nm} < 35\pi/36,$$
$$= A/\sin(\pi/36), \quad \text{otherwise}$$

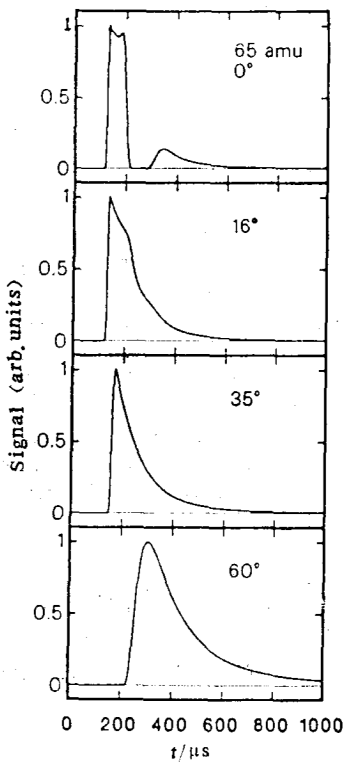

Fig. 5 TOF spectra of the secondary species 65 amu at different LAB angles

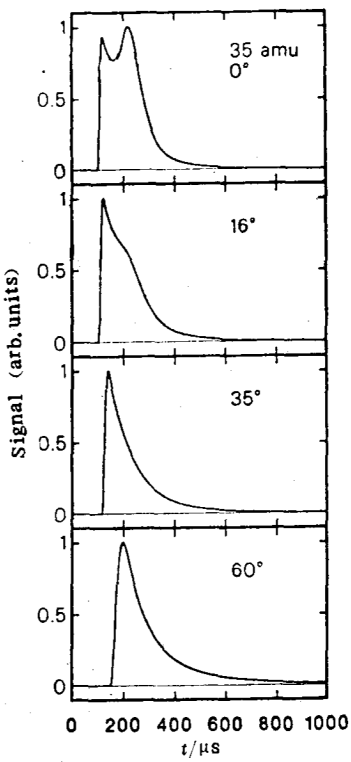

Fig. 6 TOF spectra of the secondary species 35 amu at different LAB angles

where A is a normalization constant and θ_{nm} is the angle between the primary and secondary vectors $\hat{u}_{An}$ and $\hat{u}_{\Omega nm}$. This secondary angular distribution is representative

of highly prolate fragments created by large impact parameter bond fissions which later decompose in the plane of rotation perpendicular to the orbital angular momentum. The TOF spectrum in Fig. 8 b) corresponds to

$$P_{\Omega nm}(\Omega_{nm}) = A' e^{-1/2\left(\frac{\cos\theta_{nm}}{\cos\theta_0}\right)^2}$$

where A' is a normalization constant and we have set $\cos\theta_0 = 1/2$. This distribution can qualitatively represent a fast secondary dissociation which prefers a perpendicular dissociation geometry. In the second case, the TOF spectra usually become narrower than in isotropic dissociation.

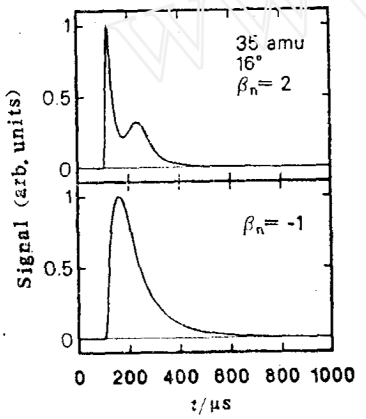

Fig. 7 The effect of anisotropic primary dissociation on the TOF spectra of the secondary products. $\beta_n = 2$ and -1 refer to transition dipoles aligned parallel and perpendicular to primary product c. m. velocity vector. See Fig. 6 for the related isotropic TOF spectrum at 16°

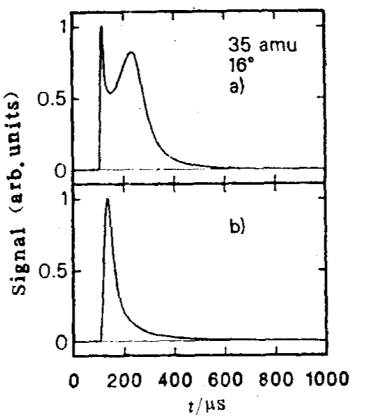

Fig. 8 The effect of anisotropic secondary dissociation on the TOF spectra of the secondary products. The spectra in a) and b) refer to enhanced dissociation with the secondary product c. m. velocity vector parallel and perpendicular to the direction of the primary product c. m. velocity vector, respectively. See Fig. 6 for the related isotropic TOF spectrum at 16°

ACKNOWLEDGEMENTS The authors wish to thank E. J. Hintsa, Q. H. Zhu, T. K. Minton, and A. M. Wodtke for helpful discussions. GMN thanks the Miller Institute of the University of California for a fellowship. This work was supported by the office of US Naval Research under Contract No. N00014-83-K-0069.

REFERENCES

[1] Wodtke, A. M., Lee, Y. T., in *"Advances in Gas Phase Photochemistry and Kinetics"*, J. Baggott and M. Ashfold, Eds., Royal Society of Chemistry, London 1987

[2] Zhao, X., Hintsa, E, J., Lee, Y. T., *J. Chem. Phys.*, 1988, 88, 801

[3] Hintsa, E. J., Wodtke, A. M., Lee, Y. T., *J. Phys. Chem.*, 1988, 92, 5379

[4] Nathanson, G. M., Minton, T. K., Shane, S. F., Lee, Y. T., *J. Chem. Phys.*, 1989, 90, 6157

[5] Kroger,P. M., Riley, S. J., *J. Chem. Phys.*, 1977, 67, 4483

[6] Kroger,P. M., Riley, S. J., *J. Chem. Phys.* 1978, 70, 3863

[7] Ray, U., Brandow, S. L., Bandukwalla,G.,Venkataraman,B. K.,Zhang,Z., Vernon,M., *J. Chem. Phys.*, 1988, 89, 4092

[8] Warnock T. T., Bernstein, R. B., *J. Chem. Phys.*, 1968, 49, 1878

[9] Pack, R. T., *J. Chem. Phys.*, 1984, 81, 1841

[10] Zhao, X., Ph. D. Thesis, University of California, Berkeley 1988

[11] Krajnovich, D., Huisken, F., Zhang, Z., Shen, Y. R.,Lee, Y. T.,*J. Chem. Phys.*1982, 77, 5977

[12] Zare, R. N., *Mol. Photochem.*, 1972, 4, 1

[13] Barnwell, J. D., Loeser, J. G., Herschbach, D.R., *J. Phys. Chem.*, 1983, 87,2781

[14] Minton, T.K., Felder, P., Brudzynski, R.J.and Lee, Y.T., *J.Chem.Phys.* 1984, 81, 1759

光解碎片平动谱中二级过程的运动学及化学动力学

赵新生* Nathanson, G. M.

(北京大学化学系 北京 100871) (威其康星大学化学系)

李远哲

(加里福尼亚大学 化学系)

摘要 本文发展了一套分析处理分子束光解反应实验中二级分解产物飞行谱的方法，它改进了Kroger和Riley的最初讨论。本文表明许多重要的信息都可以从高度平均的实验数据中得出。这包括二级分解产物的平均平动能分布、空间各向异性参数、平行竞争通道间的反应比。模拟的结果可以表现二级分解反应的一些主要特征。

关键词：数据模拟 光解 分子束 二级过程